

## P-wave upper-mantle tomography of the Tanlu fault zone in eastern China

Jianshe Lei<sup>a,\*</sup>, Dapeng Zhao<sup>b</sup>, Xiwei Xu<sup>a</sup>, Mofei Du<sup>a</sup>, Qi Mi<sup>a</sup>, Mingwen Lu<sup>a</sup><sup>a</sup> Key Laboratory of Crustal Dynamics, Institute of Crustal Dynamics, CEA, Beijing 100085, China<sup>b</sup> Department of Geophysics, Graduate School of Science, Tohoku University, Sendai 980-8578, Japan

## ARTICLE INFO

## Keywords:

Teleseismic tomography

Upper mantle structure

Tanlu fault zone

Tancheng earthquake

## ABSTRACT

The Tanlu fault zone is the most significant active fault in eastern China, which generated the great 1668 Tancheng earthquake ( $M$  8.5). It is still unclear whether or not there is a link between the great earthquake generation and the upper-mantle structure. To address this issue, we study P-wave upper-mantle tomography beneath eastern China using 44,047 teleseismic P-wave arrival times. Our results show that at depths  $< 150$  km, high-velocity (high-V) anomalies appear west of the Tanlu fault zone, whereas low-velocity (low-V) anomalies are visible east of the fault zone. Strong lateral heterogeneities are revealed along the fault zone. At depths of 230–470 km, northwest of the Tanlu fault zone, there are obvious low-V anomalies that may reflect hot and wet mantle upwelling, whereas to the east high-V anomalies are visible, which may reflect the detached Eurasian lithosphere (downwelling). In the mantle transition zone (MTZ), both high-V and low-V anomalies are revealed, and the widespread high-V anomalies may reflect the stagnant Pacific slab. Beneath the hypocenter of the 1668 Tancheng earthquake, intermittent low-V anomalies are revealed in the upper mantle down to the MTZ depth, which may reflect hot and wet mantle upwelling flow. Integrating the present results with previous findings, we deem that the Tancheng earthquake was affected by fluids from the hot and wet mantle upwelling associated with the lithospheric delamination. Complicated mantle convection, including both upwelling and downwelling flows, may occur under the Tanlu fault zone in the big mantle wedge above the stagnant Pacific slab in the MTZ.

## 1. Introduction

The Tanlu fault zone is located in the back-arc region of the western Pacific subduction zone (Fig. 1), and it is the most significant active fault zone in eastern China. Xu et al. (1993) called it the Tanlu fault zone because it was originally thought that the zone extends only from Tancheng to Lujiang. This approximately NNE-SSW-trending fault zone extends over 2400 km in the Chinese territory from Zhaoxing near the border between Russia and China through the Bohai Sea to Guangji near the northern bank of the Changjiang (Yangtze) River (e.g., Xu et al., 1987; Xu, 1993; Okay and Sengor, 1992). The Tanlu fault zone has experienced a complicated evolution process. During the late Triassic to the middle Cretaceous, it was a left-lateral strike-slip fault zone with a total displacement of  $\sim 150$ – $200$  km (e.g., Cao and Dong, 1987), or  $300$ – $400$  km (e.g., Guo, 1987; Wan and Zhu, 1996), or even to  $\sim 740$  km (e.g., Xu, 1984, 1993; Chen, 1988; Xu and Ma, 1992; Wang et al., 2000; Zhu et al., 2001, 2003). However, in the late Cretaceous period, it experienced intensive extensional activities (Zhang et al., 2003; Zhu et al., 2008) leading to a series of rifting basins, and became a strong rift-type fault that accumulated clastic and pyroclastic sediments with a thickness of up to 10 km (e.g., Xu, 1984). In the Paleogene

the rifting graben was closed as a response to a change in the orientation of regional tectonic stress from WNW extension to ENE contraction (e.g., Gao et al., 1980), and gradually evolved into a right-lateral strike-slip fault zone in the late Eocene time (e.g., Lu et al., 1983; Wang et al., 2000) due to the Indo-Asian collision (e.g., Molnar and Tapponnier, 1975; England and Houseman, 1986; England and Molnar, 1997; Yin, 2000; Zhou and Lei, 2016; He et al., 2018) and the Pacific plate subduction (e.g., Lei and Zhao, 2005, 2006; Huang and Zhao, 2006; Wei et al., 2012; Fukao and Obayashi, 2013; Chen et al., 2017).

According to its structural behaviors and evolutionary history, the Tanlu fault zone can be divided into the northern, central and southern segments, and the central segment is located at the Bohai Bay (e.g., Xu and Ma, 1992; Wang et al., 2000; Liu et al., 2015). Each segment has distinct activity modes at different times, especially to the south of the Bohai Bay. Thus, the Tanlu fault zone has obviously different features of earthquake activity. In the Shandong province, it is the most active and has the strongest seismic activities (e.g., Wu et al., 1981; Li et al., 1994; Chao et al., 1997). In this segment, the most representative example of the seismicity is the 25 July 1668 Tancheng earthquake ( $M$  8.5) that caused over 50,000 fatalities. Being affected by the Tancheng earthquake, there have been a few earthquakes in the north of Jiangsu

\* Corresponding author.

E-mail address: [jshlei\\_cj@126.com](mailto:jshlei_cj@126.com) (J. Lei).<https://doi.org/10.1016/j.pepi.2019.106402>

Received 31 August 2019; Received in revised form 15 November 2019; Accepted 15 November 2019

Available online 18 November 2019

0031-9201/ © 2019 The Authors. Published by Elsevier B.V. This is an open access article under the CC BY-NC-ND license (<http://creativecommons.org/licenses/by-nc-nd/4.0/>).

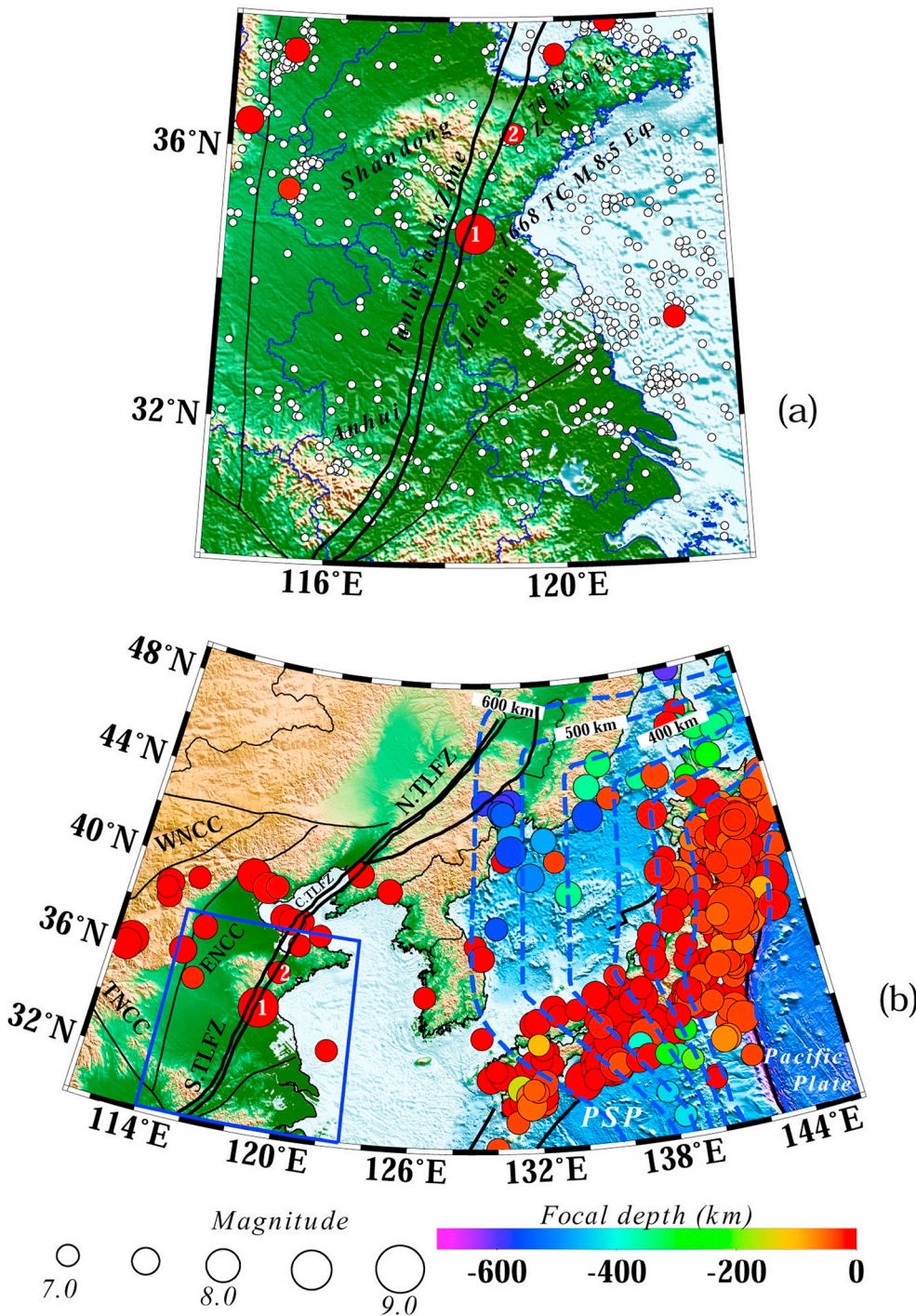


**Fig. 1.** Tectonic setting of the present study region (a) and East Asia (b). The thick black lines denote the Tanlu fault zone (TLFZ, Deng et al., 2002), whereas the thin black lines represent boundaries of the North China Craton (NCC). The color circles denote large earthquakes ( $M > 7$ ) that occurred during 1600 to 2010 (Song et al., 2011). The size and color of the circles represent the earthquake magnitude and focal depth, respectively, whose scales are shown at the bottom. The largest circles 1 and 2 in (a) denote the epicenters of the 25 July 1668 Tancheng earthquake ( $M$  8.5) and 70 BCE Zhucheng earthquake ( $M$  7.0) (Song et al., 2011). The small white dots in (a) mark the seismicity ( $M > 3$ ) during 1985 to 2005. The blue contour lines in (b) illustrate depths to the upper boundary of the subducting Pacific slab. S.TLFZ, the southern TLFZ; C.TLFZ, the central TLFZ; N.TLFZ, the northern TLFZ; WNCC, the western NCC; TNCC, the Trans NCC; ENCC, the eastern NCC; PSP, the Philippine Sea Plate. (For interpretation of the references to color in this figure legend, the reader is referred to the web version of this article.)

province. In the Anhui province, only some small earthquakes took place. Such segmental differences of the Tanlu fault zone have attracted many researchers to make various investigations, such as active-source deep seismic surveys (e.g., Liu et al., 2015; Li et al., 2011), magnetotelluric soundings (e.g., Ye et al., 2009; Zhang et al., 2010), and portable seismic observations (e.g., Chen et al., 2006, 2009), to study the crust and upper mantle structure and geodynamic processes related to the North China Craton (NCC) destruction (e.g., Zhu et al., 2011, 2012). However, these previous investigations were made along linear profiles normal to the Tanlu fault zone and so it was hard to obtain information on the three-dimensional (3-D) structure of the crust and upper mantle beneath the fault zone.

To date, a few researchers have performed seismic tomography

using arrival-time data recorded by Chinese provincial seismic networks to study the 3-D crust and upper mantle structure in eastern China, but the data used were recorded in short time periods or collected from the seismic network bulletins (e.g., Tian et al., 2009; Lei, 2012; Zhao et al., 2012), which were insufficient to obtain a high-resolution tomographic model for understanding the deep structure and dynamics of the Tanlu fault zone. For example, Tian et al. (2009) used the data selected from the Annual Bulletin of Chinese Earthquakes during 1980 to 2005, whereas Lei (2012) and Zhao et al. (2012) used arrival-time data recorded during 2007–2009 and 2007–2010, respectively.

In the present study, we have made great efforts to collect as many P-wave arrival-time data as possible from original seismograms



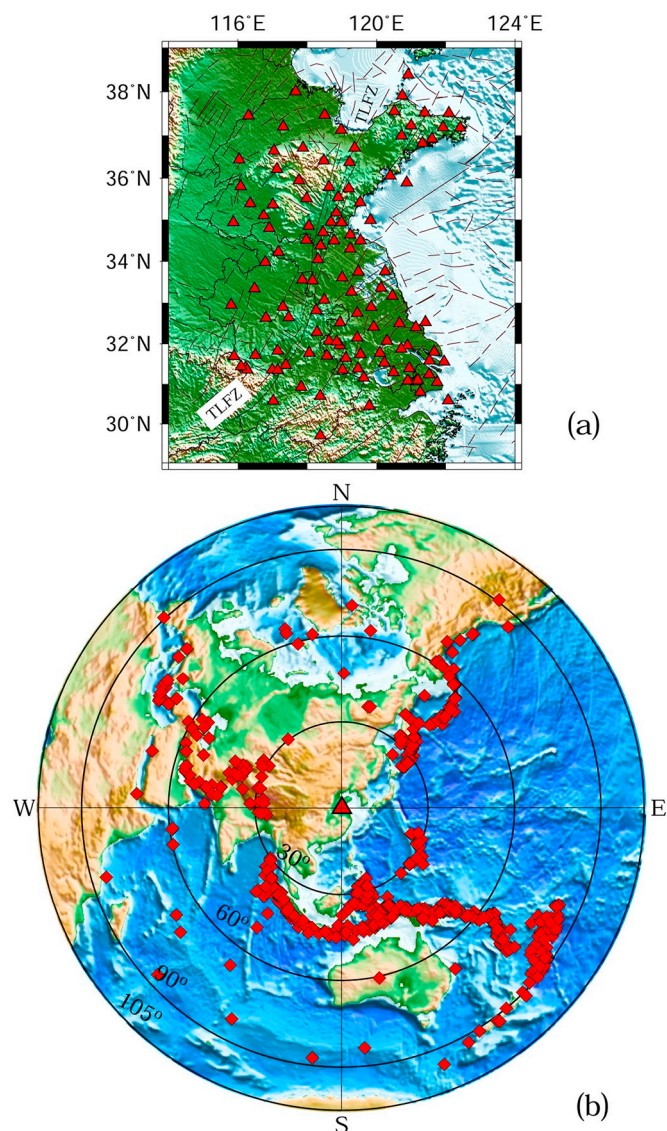


**Fig. 2.** (a) Distribution of seismic stations (red triangles) used in this study. TLFZ, the Tanlu fault zone. (b) Epicentral distribution of teleseismic events (diamonds) used in this study. The red triangle denotes the center of the study area. The concentric circles denote the equidistance (in degrees) from the red triangle. (For interpretation of the references to color in this figure legend, the reader is referred to the web version of this article.)

recorded at the Chinese provincial seismic stations (Zheng et al., 2010) during 2008 to 2016. A large number of collected data are inverted for a high-resolution 3-D model of P-wave upper-mantle tomography in and around the Tanlu fault zone. Our results shed new light on the causal mechanism of the 1668 Tancheng earthquake (M 8.5) on the Tanlu fault zone, as well as related issues of mantle dynamics in eastern China.

## 2. Data and method

In this work we carefully picked arrival-time data from high-quality seismograms recorded at 126 seismic stations that have been operated in the Shandong, Jiangsu and Anhui provinces, as well as the Shanghai district during 2008 to 2016 (Fig. 2a). These stations are distributed densely and uniformly in and around the Tanlu fault zone, which is preferable from a viewpoint of tomographic imaging. In the above-mentioned period, these stations recorded 838 teleseismic events ( $M > 5.5$ ) with epicentral distances of 30 to 90 degrees (Fig. 2b). We

can see that these events have a very good azimuthal coverage around our study region, though they mainly occurred in the western Pacific subduction zones, the Indo-Australia subduction zone, the Indo-Eurasian collision zone, and the Mid-East region. The well-distributed events (Fig. 2b) recorded by the dense seismic network (Fig. 2a) provide crisscrossing rays in the upper mantle under the study region, enabling us to determine high-resolution tomography of the study volume.

As shown in Fig. 3, our data set contains 45,127 (94.5% of the total arrivals) raw travel-time residuals (i.e., the observed minus theoretical travel times) that are within a range of  $\pm 3.0$  s and are used to calculate relative travel-time residuals (i.e., raw residuals minus the average residual of a teleseismic event over all the stations). Finally, we have 44,047 (92.3% of the total arrivals) relative residuals within a range of  $\pm 1.5$  s, which are used to conduct tomographic inversions.

We apply the tomographic method of Zhao et al. (1994) to the teleseismic data to image the 3-D upper mantle structure under the study region. Theoretical ray paths and travel times are calculated using a 3-D ray tracer (Zhao, 2001; Zhao and Lei, 2004) for a 1-D velocity model. This ray tracer can compute not only the travel times and ray paths precisely and efficiently, but also can deal with a model containing complex velocity discontinuities, such as the Moho and a subducting slab boundary. The crustal part of the 1-D velocity model is constructed by averaging the velocities in the CRUST1.0 model (Laske et al., 2012) and the models of the Moho discontinuity by He et al. (2014), Li et al. (2014) and Teng et al. (2014). For the upper mantle, the 1-D IASP91 velocity model (Kennett and Engdahl, 1991) is adopted. We use the relative travel-time residuals of the teleseismic events to conduct tomographic inversions so as to avoid the effect of uncertainties in the hypocentral parameters and structural heterogeneities outside the study volume on the tomographic result under the study region. For more details, see Zhao et al. (1994) and Lei and Zhao (2005). To remove the effect of crustal heterogeneities on the upper-mantle tomography, we make crustal corrections to the relative travel-time residuals using a 3-D crustal model. This 3-D crustal model is constructed by directly adopting velocities in the CRUST1.0 model (Laske et al., 2012) and a Moho geometry that is derived by averaging the models of He et al. (2014), Li et al. (2014), and Teng et al. (2014).

A 3-D grid is set up in the study volume to express the P-wave velocity ( $V_p$ ) structure. Our 3-D  $V_p$  model is parameterized with an optimal lateral grid interval of  $0.7^\circ \times 0.7^\circ$  and with grid meshes arranged at depths of 70, 150, 230, 310, 390, 470, 550, 630, and 710 km, after performing many checkerboard resolution tests with various grid intervals in the horizontal and vertical directions.  $V_p$  perturbations at the grid nodes are taken as unknown parameters that are resolved by inversion when the ray hit counts at the nodes are larger than 10. A conjugate-gradient type algorithm LSQR (Paige and Saunders, 1982) with damping and first-order smoothing regularizations is used to resolve the large and sparse systems of observational equations (Zhao, 2001; Lei and Zhao, 2006). The optimal value of the damping parameter is found to be 20.0 from the balance between the reduction of travel-time residuals and the smoothness of the 3-D  $V_p$  model, after performing many tomographic inversions with different values of the damping parameter (Fig. 4). In a similar way, the optimal values of the horizontal and vertical smoothing parameters are determined, both of which are 0.025.

## 3. Resolution analysis and results

### 3.1. Resolution analysis

Checkerboard resolution tests (CRTs) are usually performed to examine the reliability and resolution scale of an obtained tomographic model. To conduct a CRT, negative and positive  $V_p$  anomalies of up to 2% relative to the 1-D  $V_p$  model are alternately assigned to the 3-D grid nodes in the input model. The numbers of seismic stations, events, and

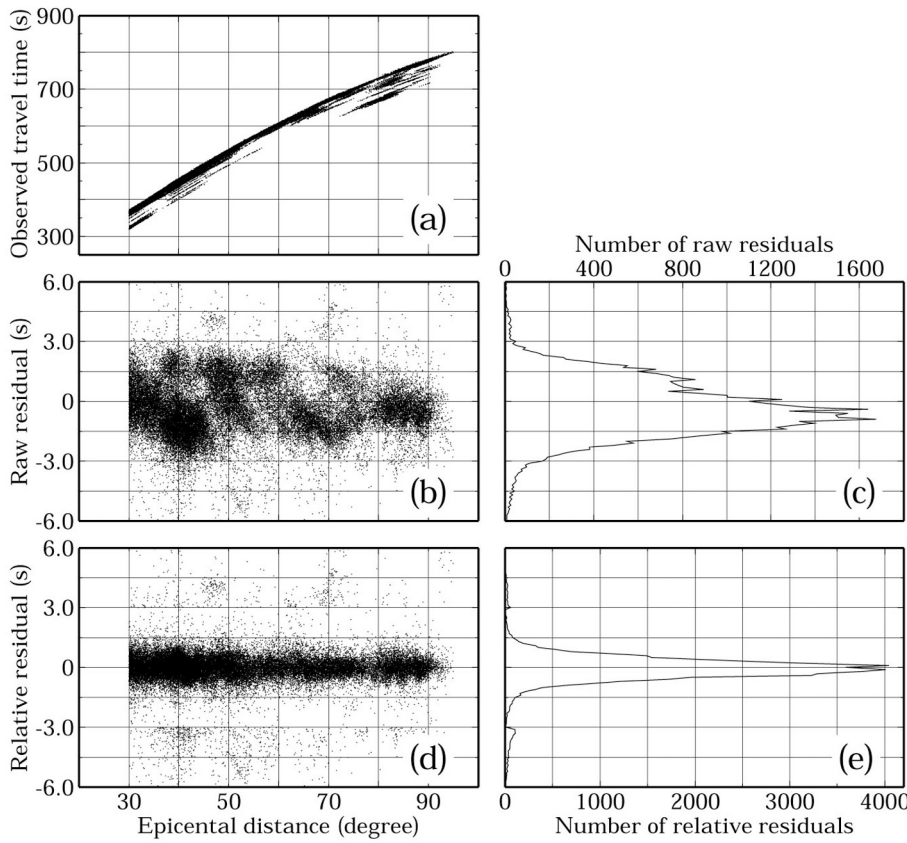


**Fig. 3.** (a) The observed P-wave travel times (in second) versus epicentral distance between 30 and 95°. (b) Raw travel-time residuals versus epicentral distance (in degree). (c) Histogram of the raw residuals. (d) Relative travel-time residuals versus epicentral distance. (e) Histogram of the relative residuals. See the text for details.

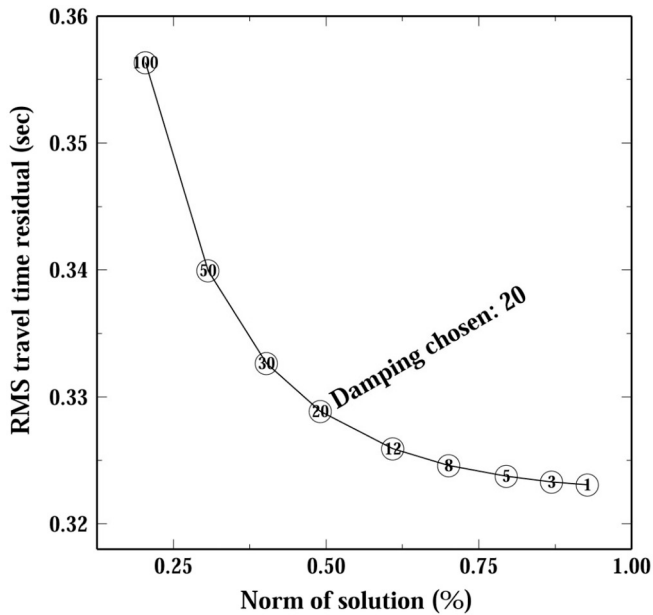


**Fig. 4.** Trade-off curve for the root-mean-square (RMS) travel-time residuals versus norm of solution. Numbers inside the open circles denote the damping parameters. The optimal damping parameter (20.0) is determined to obtain our preferred tomographic model.

ray paths are the same as those in the real data set. Random noise ( $-0.2$  s to  $+0.2$  s) with a zero mean and a standard deviation of  $0.1$  s is added to synthetic travel times calculated for the input checkerboard model to account for the picking errors ( $\sim 0.1$  to  $0.2$  s) of the travel-time data. The synthetic data are then inverted to get a recovered image of the checkerboard model using the same inversion method as mentioned

in Section 2. The resolution is considered to be good for those areas where the checkerboard image is retrieved.

Many CRTs are conducted with different grid intervals in the input model. Fig. 5 shows results of one CRT we performed with a lateral grid interval of  $0.7^\circ \times 0.7^\circ$  and a vertical grid interval of  $80$  km. At  $70$  km depth (Fig. 5a), the well-resolved area is consistent with the distribution of seismic stations (Fig. 2a). The area with good resolution becomes gradually wider with depth (Fig. 5b–e). However, in the mantle transition zone (MTZ) the well-resolved area gets gradually smaller and moves eastward (Fig. 5f–i), mainly because most of the rays come from the western Pacific subduction zones (Fig. 2b). The CRT results suggest that  $V_p$  anomalies with a size of  $> \sim 70$  km in our tomography are reliable features.

### 3.2. Tomographic results

Fig. 6 shows map views of our obtained  $V_p$  tomography. At  $70$  km depth, to the west of the Tanlu fault zone, there are obvious high-velocity (high-V) anomalies, whereas to the east an obvious low-velocity (low-V) anomaly is visible (Fig. 6a). Along the fault zone, pronounced lateral heterogeneities exist. The 1668 Tancheng earthquake ( $M$  8.5) occurred at the margin of high-V anomalies, whereas some low-V anomalies are imaged in the areas where some conjugated fault zones exist (Fig. 6a). This pattern of velocity anomalies extends down to a depth of  $150$  km, but there are some subtle differences. At a depth of  $150$  km, to the west and east of the Tanlu fault zone, both high-V and low-V anomalies move southward (Fig. 6b). Furthermore, on the fault zone a low-V anomaly appears around the 1668 Tancheng epicenter (Fig. 6b). At a depth of  $230$  km, there is no obvious pattern of  $V_p$  anomalies (Fig. 6c), but down to depths of  $310$ – $470$  km there is a striking feature (Fig. 6d–f). An obvious low-V anomaly is visible to the northwest of the Tancheng epicenter, whereas high-V anomalies appear to the southeast. At depths of  $550$ – $710$  km, significant high-V and low-V anomalies are clearly visible (Fig. 6g–i), where the high-V anomalies



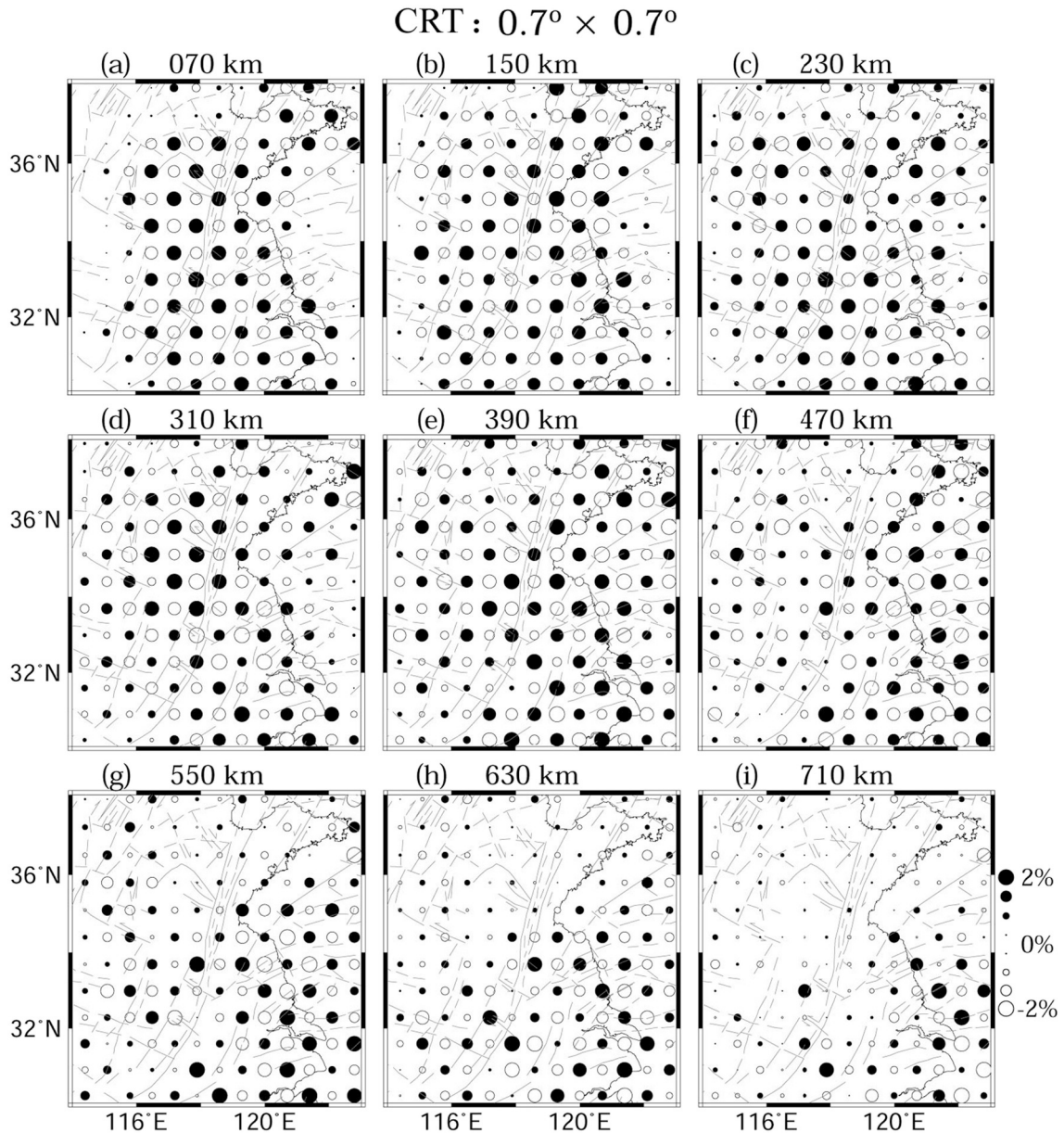


**Fig. 5.** Results of a checkerboard resolution test with a lateral grid interval of  $0.7^\circ \times 0.7^\circ$ . The layer depth is shown above each map. The open and solid circles denote low-V and high-V anomalies, respectively, whose scale (in %) is shown on the right. The thin lines denote the major active faults (Deng et al., 2002).

may reflect the stagnant Pacific slab in the MTZ, whereas the low-V anomalies may reflect hot materials upwelling from the lower mantle. The hot mantle upwelling may be caused by the slab collapsing down to the lower mantle due to the gravitational instability from the spinel-perovskite mineral phase transformation at  $\sim 660$  km depth. The phase change at the 660 km discontinuity may cause the slab to first stagnate in the MTZ and then eventually penetrate to the lower mantle when a sufficient amount of slab material has accumulated in the MTZ (e.g., Machetel and Weber, 1991; Honda et al., 1993; Cadek et al., 1994) or the slab tearing-off occurs from the trench retreat (e.g., Yang et al., 2018).

To clearly illustrate the mantle structural features around the Tanlu fault zone, we present six east-west vertical cross-sections of the Vp tomography across the fault zone (Fig. 7). It can be seen that there are obvious differences in the structural features between the north and south of the 1668 Tancheng earthquake hypocenter. To the north, in the upper mantle obvious low-V anomalies are visible extending upward to the west of the Tanlu fault zone, and in the MTZ there are high-

V anomalies reflecting the subducted Pacific slab (Fig. 7a–c). However, to the south of the Tancheng epicenter, we can see low-V anomalies above 200 km depth and high-V anomalies at depths of 200–500 km to the east of the Tanlu fault zone (Fig. 7d–f). These Vp discrepancies across the Tancheng epicenter might indicate different effects of the stagnant Pacific slab in the MTZ due to a sharp change in the subduction direction and dip angle of the subducting slab from the Japan trench to the Izu-Bonin trench (e.g., Obayashi et al., 2009). This issue requires further investigations by further studies.

To better understand the deep structural features around the 1668 Tancheng source area, we show two more vertical cross-sections of Vp tomography passing through the earthquake hypocenter (Fig. 8). Above 100 km depth, high-V anomalies are imaged around the hypocenter, but below 100 km depth obvious low-V anomalies exist down to the MTZ. In the lower part of the MTZ, prominent high-V anomalies are revealed, which may reflect the stagnant Pacific slab (Fig. 8a–b).

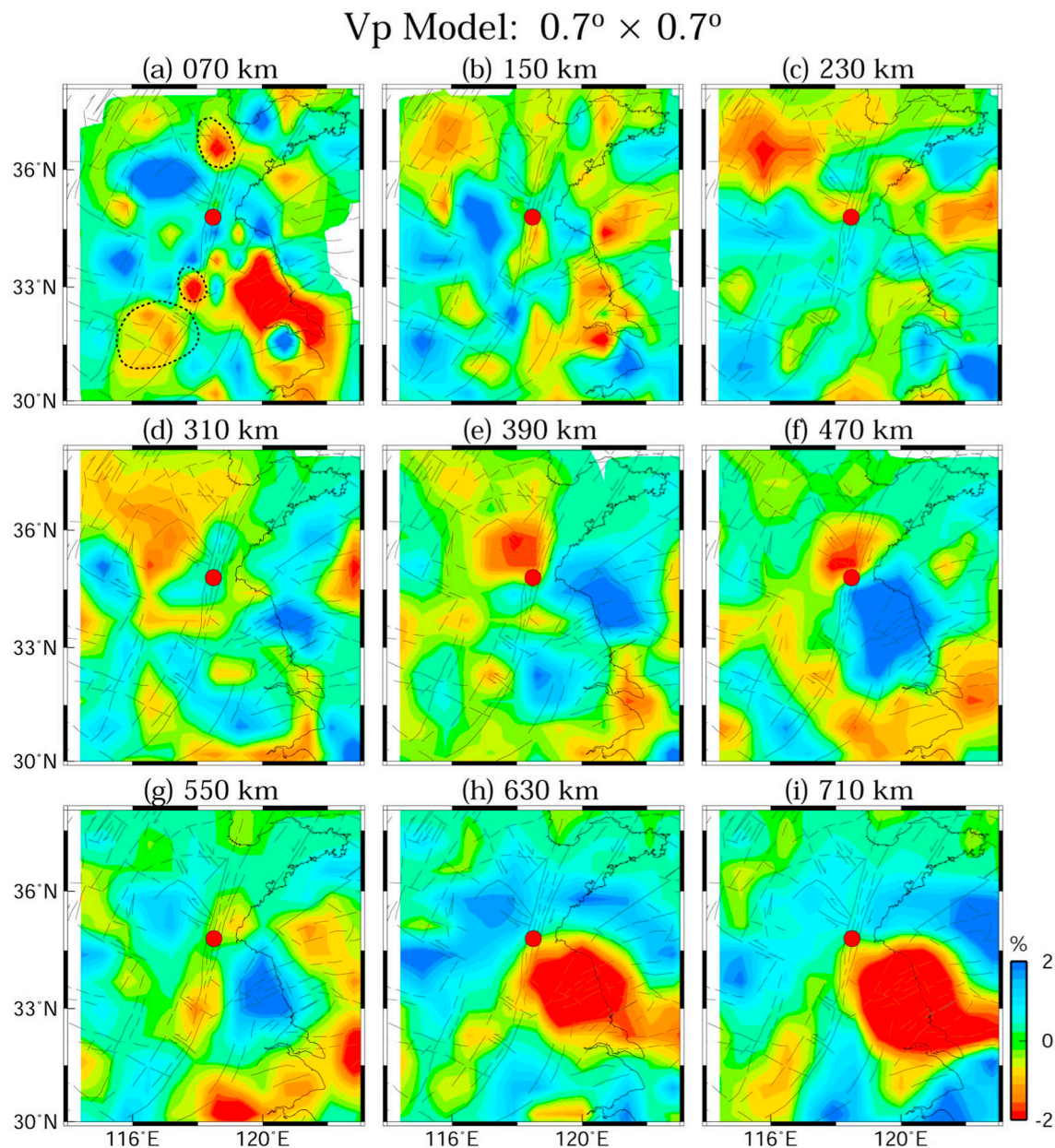


**Fig. 6.** Map views of P-wave velocity ( $V_p$ ) tomography obtained by this study. The layer depth is shown above each map. The red and blue colors denote low- $V$  and high- $V$  anomalies, respectively, whose scale (in %) is shown on the right. The red dot denotes the epicenter of the 1668 Tancheng earthquake ( $M$  8.5). The thin black lines denote major active faults (Deng et al., 2002). The thick dashed circles in (a) mark conjugate fault zones. (For interpretation of the references to color in this figure legend, the reader is referred to the web version of this article.)

### 3.3. Effect of the crustal correction

Teleseismic rays are nearly vertical and so do not crisscross in the crust, which may cause leakage of the crustal heterogeneity to the upper mantle, and vice versa. To avoid such effects, in the present study we use the existing 3-D crustal model as mentioned in Section 2 to correct the teleseismic relative travel-time residuals (Fig. 8a–b). Many previous studies of teleseismic tomography have investigated this issue (e.g., Lei and Zhao, 2005, 2007; Jiang et al., 2015). Here we only compare the upper-mantle tomographic images obtained with and without the crustal correction (Fig. 8). Although the pattern of velocity anomalies remains the same, there are subtle differences in the amplitude, especially above 200 km depth (Fig. 8). Therefore, in future studies a more detailed 3-D crustal model should be determined so as to obtain a better model of the upper-mantle tomography under the Tanlu fault zone.

### 3.4. Synthetic tests

To further confirm the reliability of structural features in the tomographic model, we carry out a series of synthetic tests (e.g., Zhao, 2001; Lei and Zhao, 2005, 2006) by randomly setting up the location, size and morphology of velocity anomalies. The procedure of the synthetic tests is the same as that of the CRTs, but different input models are adopted. In a synthetic test, some specific anomalies are put in the input model. Due to the limited space of this paper, here we only show two synthetic tests (Figs. 9 and 10). In the first test, the input model contains high- $V$  and low- $V$  anomalies of up to 2% with random locations, sizes and morphologies at 230 and 310 km depths and broad high- $V$  anomalies at 550 and 630 km depths, as well as a low- $V$  anomaly to the southeast of the Tancheng earthquake (Fig. 9a–e). In the second test, we put opposite velocity anomalies at 230 and 310 km depths and only high- $V$  anomalies at 550 and 630 km depths in the



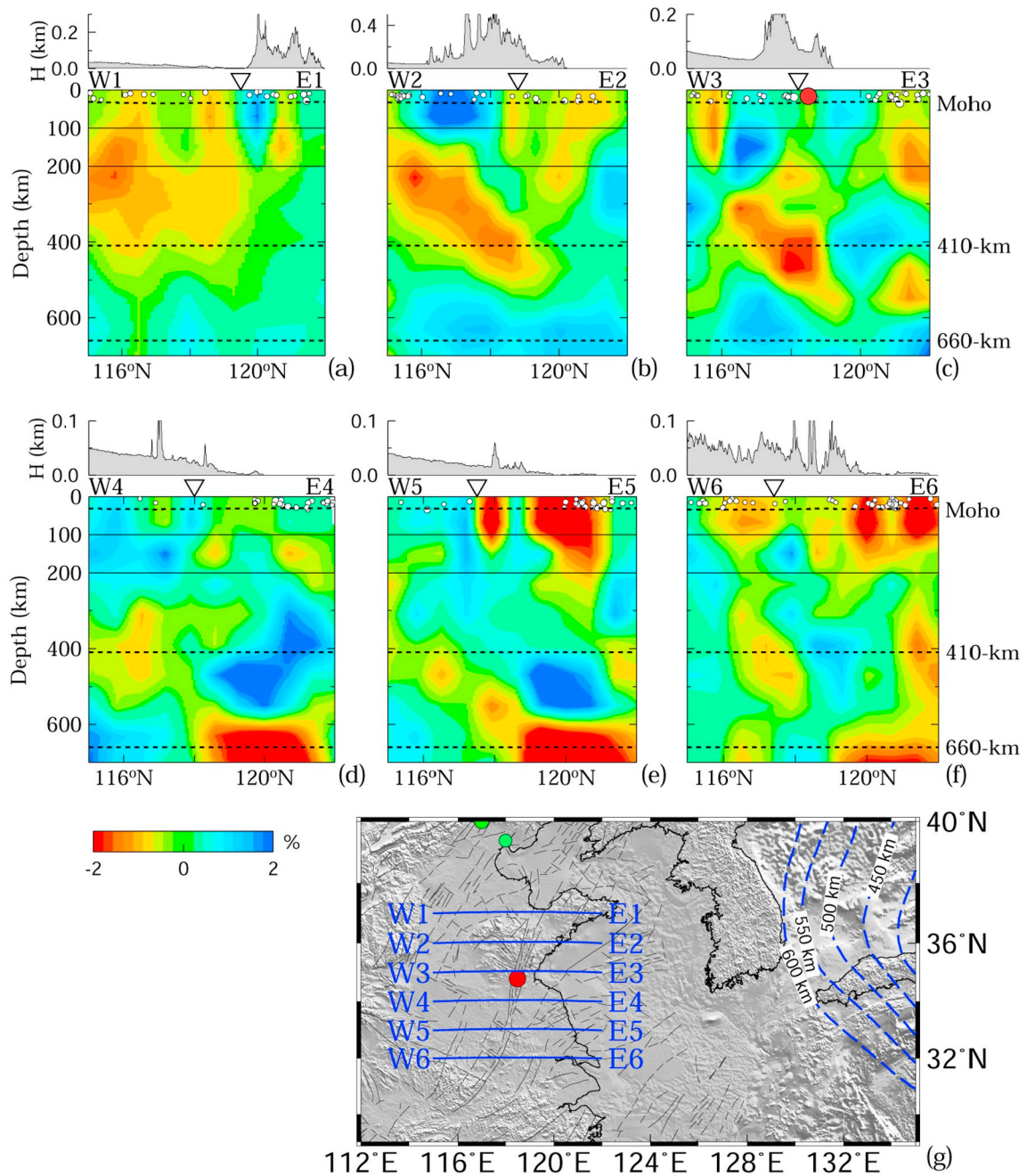


**Fig. 7.** East-west vertical cross-sections of P-wave velocity ( $V_p$ ) tomography along six profiles across the Tanlu fault zone, as shown in the inset map (g). The red and blue colors denote low-V and high-V anomalies, respectively, whose scale (in %) is shown under the profiles. The surface topography along each profile is shown above each panel. The reverse triangle denotes the location of the Tanlu fault zone. The red dot represents the hypocenter of the 1668 Tancheng earthquake (M 8.5). The small white dots denote local seismicity that occurred within a 35-km width of each profile. The three dashed lines denote the Moho, 410 and 660 km discontinuities, whereas the two solid lines mark 100 and 200 km depths. (For interpretation of the references to color in this figure legend, the reader is referred to the web version of this article.)

input model (Fig. 10a–e). The test results (Figs. 9j–j and 10j–j) show that the amplitude of velocity anomalies is not fully recovered and some smearing appears, but the pattern of velocity anomalies is reconstructed quite well. These results indicate that the main structural features are robust, such as the low-V anomaly in the MTZ to the southeast of the Tancheng epicenter.

## 4. Discussion

### 4.1. Effect of seismic anisotropy

Seismic anisotropy is a very important parameter for better understanding the dynamic processes in the Earth's interior (e.g., Long and Becker, 2010; Fouch and Rondenay, 2006). The anisotropy in the upper mantle is generally considered to be caused by the strain-induced crystallographic preferred orientation of olivine, which could be associated with mantle flow (Karato et al., 2008). Hence, seismic anisotropy can provide direct information on the dynamical processes in the big

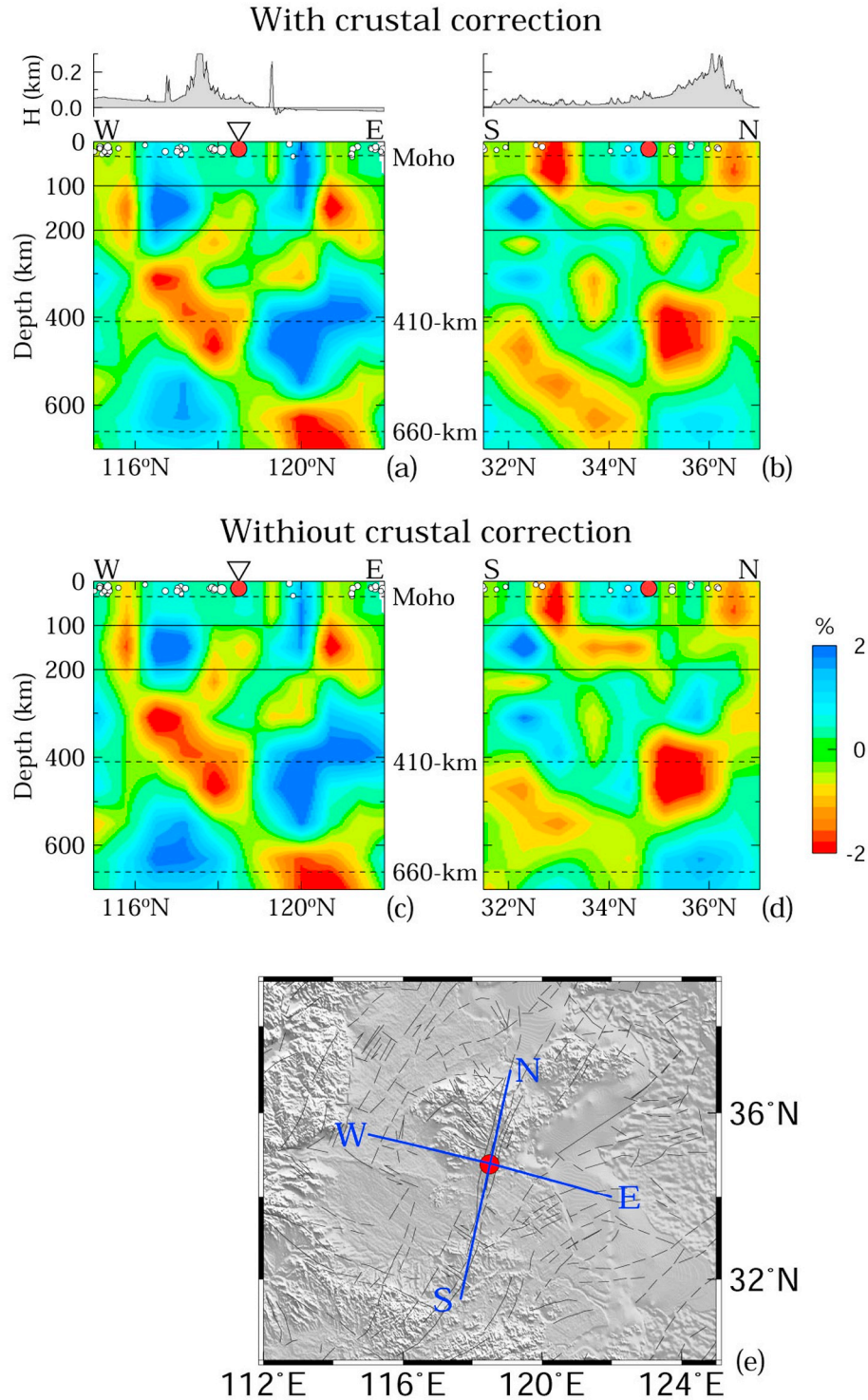


**Fig. 8.** (a–b) The same as Fig. 7 with the 3-D crustal correction but along two more profiles passing through the epicenter of the 1668  $M$  8.5 Tancheng earthquake (red dot). One profile (E–W) is perpendicular to the Tanlu fault zone, whereas the other (N–S) is along the fault zone. (c–d) The same as (a–b) but for the tomographic images without the 3-D crustal correction. The three dashed lines denote the Moho, 410 and 660 km discontinuities, whereas the two solid lines mark 100 and 200 km depths. (For interpretation of the references to color in this figure legend, the reader is referred to the web version of this article.)

mantle wedge (BMW) under eastern China. Recent studies of P-wave anisotropic tomography have shown that complex anisotropic anomalies exist in wide areas in the crust, mantle wedge and the subducting Pacific slab beneath Japan (e.g., [Ishise and Oda, 2005](#); [Wang and Zhao, 2008](#); [Liu and Zhao, 2016](#)), East China ([Tian and Zhao, 2013](#); [Huang et al., 2014](#); [Wei et al., 2016](#)), and Alaska ([Tian and Zhao, 2012](#); [Gou et al., 2019](#)). The anisotropic tomography can better reveal the crust

and upper-mantle structure under a study region because it inverts for both seismic anisotropy and 3-D velocity heterogeneity, which have the same-order effects on travel times of seismic waves ([Zhao et al., 2016](#)). In the anisotropic tomographic inversion, although anisotropy is coupled with velocity heterogeneity, their trade-off can be resolved using a good data set with dense and crisscrossing ray paths (e.g., [Huang et al., 2015](#); [Zhao et al., 2016](#)). Recent numerical simulations and practical



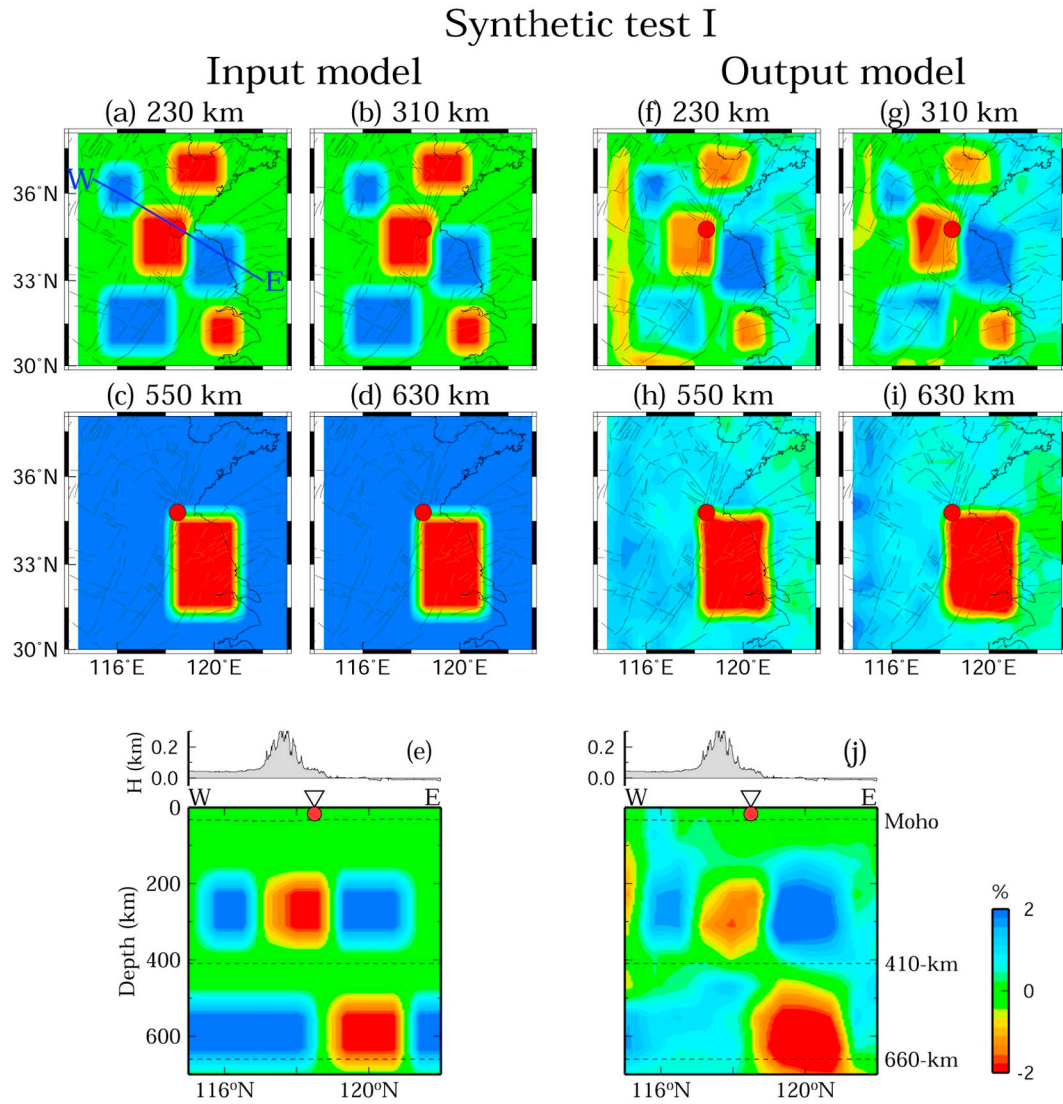


**Fig. 9.** The results of a synthetic test for high-V and low-V anomalies randomly located at 230 and 310 km depths with different sizes and morphologies and high-V anomalies at 550 and 630 km depths as well as a low-V anomaly to the southeast of the Tancheng earthquake (red dot). Right (a–e) and left (f–j) panels show input and output models, respectively. (a–d, f–i), map views; (e, j), vertical cross-section. Red and blue colors denote low-V and high-V anomalies, whose scale is shown on the right of (j). Location of the vertical cross-section is shown in (a). The dashed lines in (e) and (j) indicate the Moho and 410-km and 660-km discontinuities. The inverted triangle in (e) and (j) marks the Tanlu fault zone. (For interpretation of the references to color in this figure legend, the reader is referred to the web version of this article.)

applications showed that, although the models of isotropic tomography and anisotropic tomography have some differences in the amplitude of velocity anomalies, their patterns of isotropic  $V_p$  variations are very similar (e.g., Huang et al., 2015; Wei et al., 2016; Zhao et al., 2016). Therefore, although our present 3-D  $V_p$  model is obtained by isotropic tomography, the main features of velocity heterogeneity under the study region are considered to be quite reliable.

#### 4.2. Comparison with previous tomographic models

So far several models of the upper-mantle tomography have been obtained around the Tanlu fault zone (Fig. 11; e.g., Tian et al., 2009; Lei, 2012; Zhao et al., 2012). To determine their tomographic models, Tian et al. (2009) collected arrival-time data from the Annual Bulletin of Chinese Earthquakes, Lei (2012) manually picked arrival times from high-quality seismic waveforms, whereas Zhao et al. (2012) obtained their arrival time data using a multi-channel cross-correlation technique (VanDecar and Crosson, 1990). The former two inverted for their models applying the ray-theory tomographic technique of Zhao et al.

(1994), whereas the latter used the finite-frequency tomographic method of Hung et al. (2004). Nevertheless, these models exhibit similar patterns of velocity anomalies. Both models of Lei (2012) and Zhao et al. (2012) show some low-V anomalies in the upper mantle around the Tancheng earthquake area above 200 km depth (Fig. 11b and c), and Lei (2012) and the present model illustrate low-V anomalies around 118°E at 200–500 km depths (Fig. 11b and d). Furthermore, all these models show pronounced high-V anomalies in the MTZ (Fig. 11). However, these models are subtly different. The model of Tian et al. (2009) shows less heterogeneities in the upper mantle (Fig. 11a), whereas the other models of Lei (2012), Zhao et al. (2012), and our present study show more heterogeneities in the upper mantle (Fig. 8b–d). To the west of the Tanlu fault zone, the models of Tian et al. (2009) and Zhao et al. (2012) reveal some high-V anomalies at 200–400 km depths (Fig. 11a and c), the model of Lei (2012) and our present model show an obvious low-V anomaly (Fig. 11b and d). In addition, the model of Tian et al. (2009) only shows a strong high-V anomaly to the east of 118°E in the MTZ (Fig. 8a), whereas the models of Lei (2012), Zhao et al. (2012) and our present study show high-V

## Synthetic test II

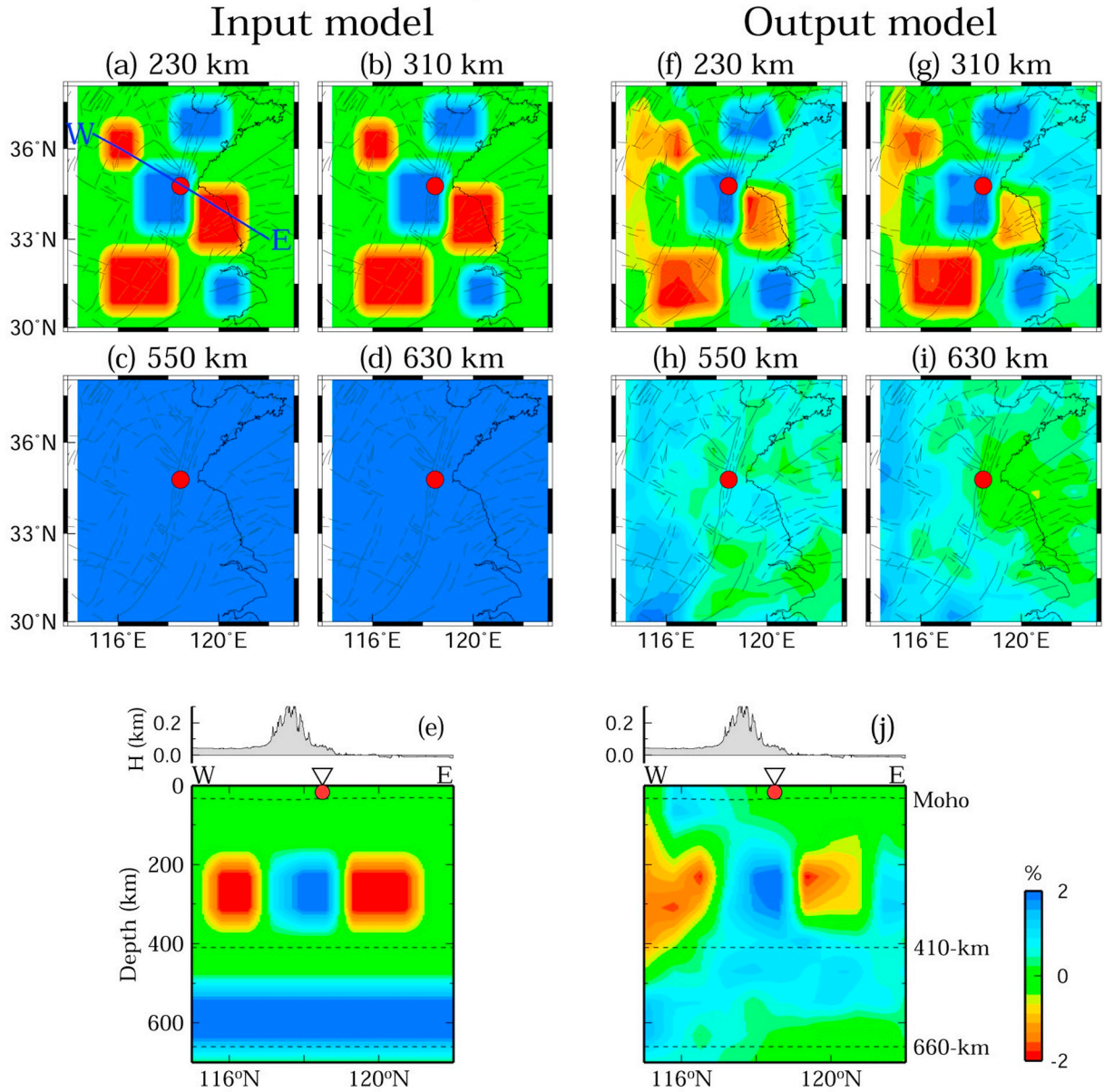


Fig. 10. The same as Fig. 9 but for opposite velocity anomalies at 230 and 310 km depths and only high-V anomalies at 550 and 630 km depths.

anomalies to the west of 120°E, to the east of 116°E, and in the range of 116°E–118°E (Fig. 11b–d), respectively. These differences may be due to the different datasets, sizes of the study volume, tomographic techniques, and regularizations adopted for the tomographic inversions. Our present model reveals more detailed structural features under the Tanlu fault zone (Fig. 11d) than the other three models (Fig. 11a–c), thanks to the better data set used in this study.

### 4.3. The Tanlu fault zone

The Tanlu fault zone is considered as a good place to study the destruction of the NCC. Many geochemical, petrological, and geophysical investigations focused on the NCC destruction in the past three decades (e.g., Menzies et al., 1993; Griffin et al., 1998; Fan et al., 2000; Xu, 2001; Wu et al., 2005; Chen et al., 2006; Tian et al., 2009; Xu and Zhao, 2009; Zhu et al., 2011, 2012; Lei, 2012; Zhao et al., 2012). These studies showed that during the late Mesozoic, the eastern NCC experienced intensive lithospheric extension, high heat flow and voluminous

magmatism, suggesting that the thick cratonic lithosphere in the region lost a significant portion of its deep mantle keel. Some researchers suggested that the NCC destruction was caused by the thermo-mechanical erosion due to the asthenospheric upwelling (e.g., Griffin et al., 1998; Xu, 2001) or a mantle plume (e.g., Lei, 2012), whereas others indicate that it can be caused by the lithospheric delamination (e.g., Gao et al., 2002; Wu et al., 2008). Nevertheless, the destructive mechanism is still under debate. A receiver-function analysis by Chen et al. (2006) showed a ~60–80 km thick present-day lithosphere around the Tanlu fault zone, which is much thinner than the Paleozoic lithosphere with ~180 km thickness. Furthermore, both the Moho discontinuity and lithosphere-asthenosphere boundary are uplifted right under the Tanlu fault zone (Chen et al., 2006). Previous tomographic models illustrate obvious low-V anomalies under the Tanlu fault zone at 50–260 km depths (Fig. 11a and c) (e.g., Tian et al., 2009; Zhao et al., 2012), indicating that the Tanlu fault zone may have acted as a major channel of hot asthenospheric mantle upwelling during the Mesozoic-Cenozoic continental extension and lithospheric thinning in



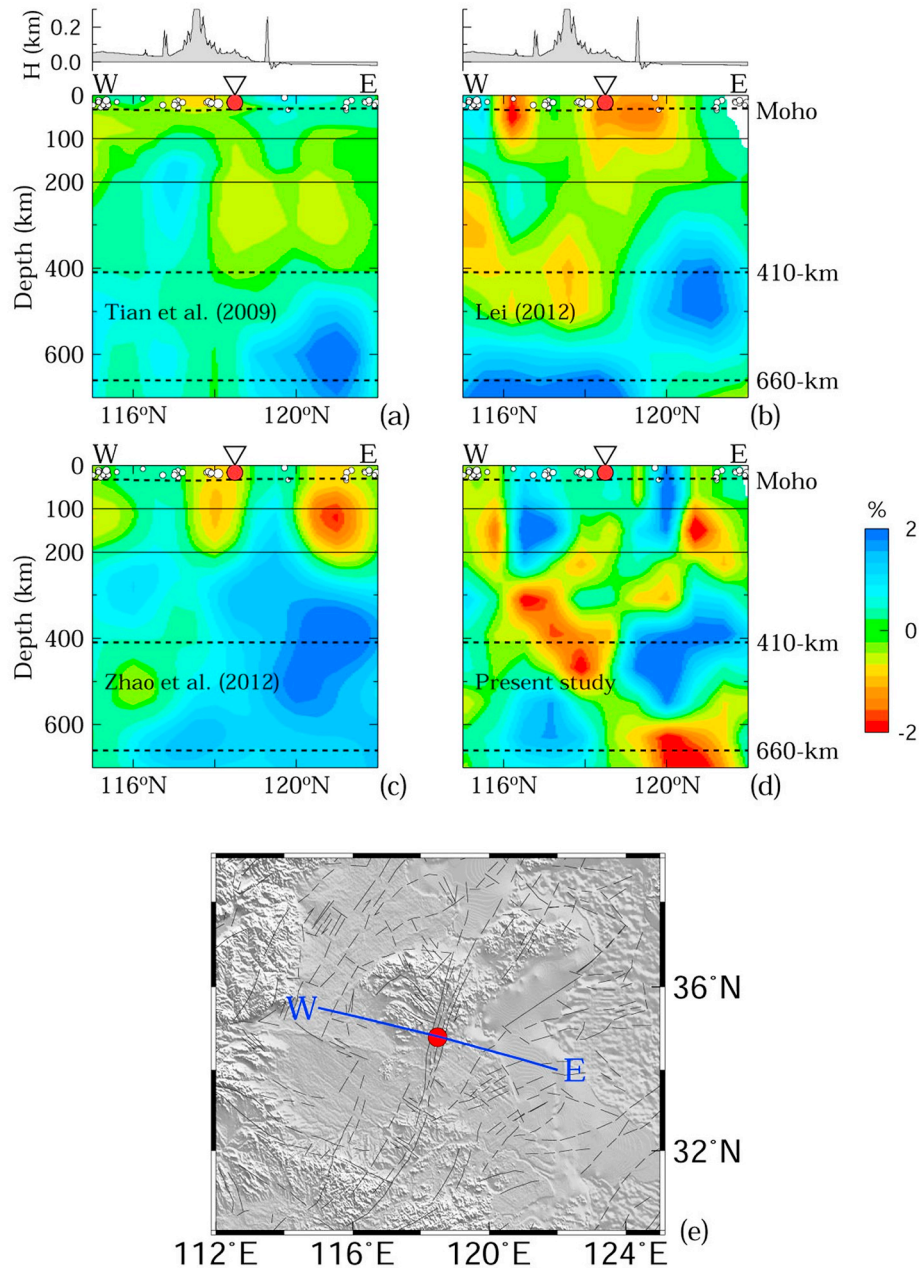


**Fig. 11.** Comparison of the previous tomographic models by (a) Tian et al. (2009), (b) Lei (2012) and (c) Zhao et al. (2012) with our present tomographic model (d). Location of the profile is shown in the inset map (e). The other labeling is the same as that in Fig. 7.

eastern China. However, our present high-resolution tomographic model shows that intermittent low-V anomalies extend upward from the MTZ (Figs. 6–8), which is supported by the previous tomographic model as shown in Fig. 11b (e.g., Lei, 2012). Furthermore, our present model also reveals some sporadic small-sized high-V anomalies below 100 km depth in the upper mantle and the MTZ (Figs. 6 and 7). These results imply that the hot and wet mantle upwelling could be associated with the lithospheric delamination (small-sized high-V anomalies) in the upper mantle and dehydration of the stagnant Pacific slab in the MTZ. Therefore, we suggest that the NCC destruction is related to the lithospheric delamination and thermal erosion due to the hot and wet mantle upwelling in the BMW.

#### 4.4. Mechanism of the *M* 8.5 Tancheng earthquake

In mainland China, many strong earthquakes have occurred in the

past decades. The recent ones are the 1976 Tangshan earthquake (*M*s 7.6) in North China, and the 2008 Wenchuan earthquake (*M*s 8.0) and 2013 Lushan earthquake (*M*s 7.0) in southwest China. The conditions that enable the generation of such large earthquakes are much more localized and determined by fault structure itself, such as the lack of asperities that enables very long ruptures to propagate unimpeded (e.g., Wang and Bilek, 2011). In these earthquake source zones, significant low-V anomalies are found in the crust (e.g., Huang and Zhao, 2004; Lei et al., 2008, 2014, 2018a; Lei and Zhao, 2009). Similar crustal structures are also found in large earthquake source zones of other regions in the world, such as the 1995 Kobe earthquake (*M*s 7.2) in SW Japan (Zhao et al., 1996) and the 2001 Bhuj earthquake (*M*s 7.6) in India (Mishra and Zhao, 2003). These results suggested that the nucleation of large crustal earthquakes could be affected by crustal heterogeneities, but few researchers mentioned that the earthquake generation could be also related to the upper-mantle structure beneath the source zones.

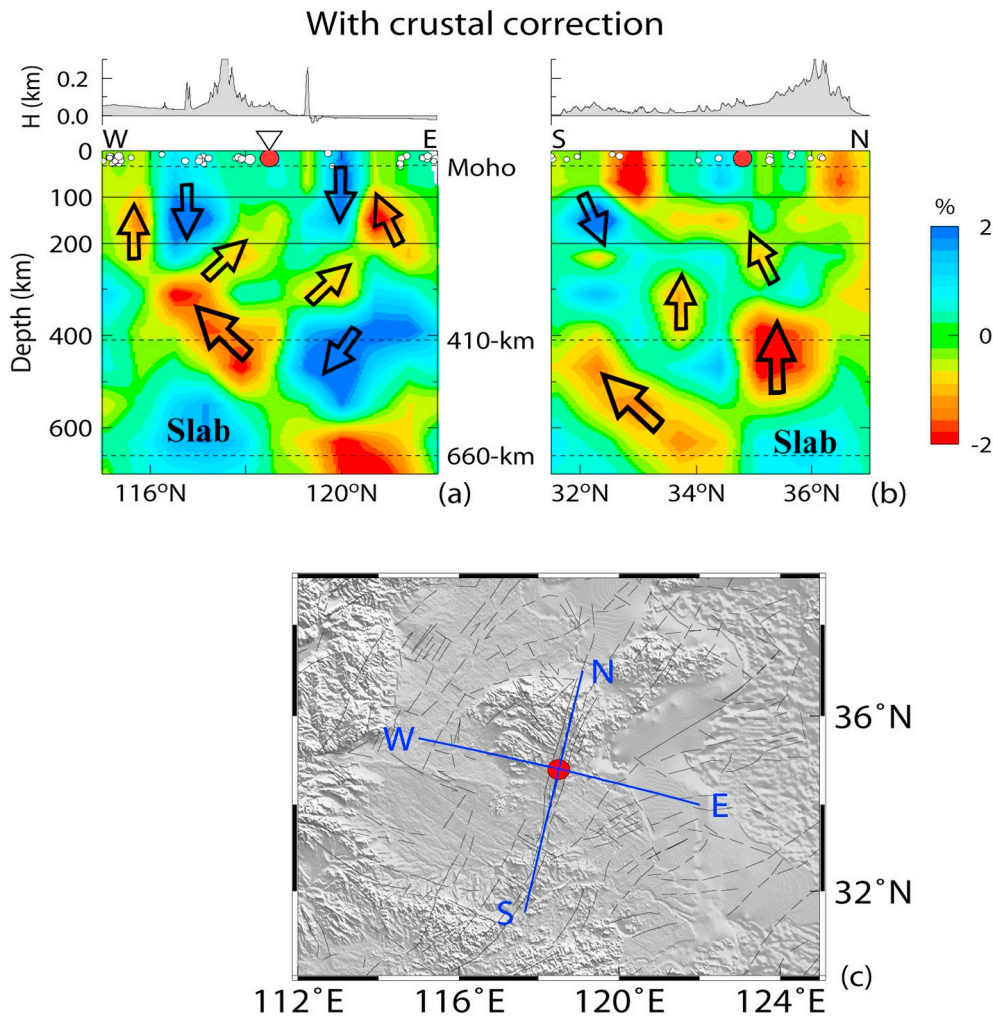


Fig. 12. The same as Fig. 8a and b but with our interpretations. The black arrows show possible directions of mantle flow. See the text for details.

In our present study, using abundant high-quality P-wave arrival-time data (Figs. 2 and 3), we reveal obvious low-V anomalies in the upper mantle down to the MTZ under the Tanlu fault zone (Figs. 6–8). These low-V anomalies could denote a channel for the wet and hot material upwelling from the MTZ (Figs. 6–8) in the BMW associated with the deep subduction and dehydration of the stagnant Pacific slab in the MTZ (e.g., Lei and Zhao, 2005, 2006; Huang and Zhao, 2006; Zhao et al., 2007, 2009; He, 2017). The upwelling flow could bring sufficient fluids, which could penetrate through the weakened lithosphere under the Tanlu fault zone and enter the crust. The over-pressurized, fluid-filled, fractured rock matrices in the crust (Zhao et al., 1996) might have contributed to the initiation of these large earthquakes. The existence of the over-pressurized fluids under the source areas has been extensively demonstrated (e.g., Johnson and McEvilly, 1995; Miller, 1996), which could affect the long-term structural and compositional evolution of the fault zone, change the fault zone strength, and alter the local stress regime (Sibson, 1982, 1992; Hickman et al., 1995). These influences may have enhanced stress concentration in the seismogenic layer, resulting in mechanical failure of the fault zone and so nucleation of the great Tancheng earthquake. On the other hand, this kind of steady-state input of fluids into the fault zone could lead to relatively weak faults, because of lubrication of the fault interface by weak hydrated minerals, increased pore pressure, or both, leading to the decrease of the frictions across the fault planes to trigger earthquakes (e.g., Bruhn and Schultz, 1996). One more example for the crustal fluids around the source areas from the upper mantle is the 1995 Kobe earthquake, which was associated with the dehydration of the

subducting Philippine Sea slab at 50–60 km depths (Zhao et al., 1996, 2002). However, we cannot rule out other sources of fluids in the crust, such as dehydration of hydroxyl-bearing minerals in the crust and fluids trapped in pore space (e.g., Zhao et al., 2002; Lei et al., 2012).

#### 4.5. Mantle dynamics

Fig. 12 shows some high-V anomalies below 100 km depth in the upper mantle, which can be interpreted as the delaminated lithosphere (blue patches with downward arrows), and some low-V anomalies in the upper mantle and in the upper part of the MTZ, which indicate hot and wet mantle upwelling (red patches with upward arrows). These results imply that complicated mantle convection takes place under the Tanlu fault zone in the upper mantle. High-V anomalies in the lower part of the MTZ represent the stagnant Pacific slab (Fig. 12), which has been imaged clearly by previous large-scale tomographic studies (e.g., Huang and Zhao, 2006; Tian et al., 2009; Lei, 2012; Li and van der Hilst, 2010; Wei et al., 2012; Zhao et al., 2012). This feature has been supported by the deeper 660 km discontinuity under the region (e.g., Shen et al., 2008). These results provide clear evidence for the destruction of the NCC that could be caused by the lithospheric delamination and thermal erosion due to asthenospheric upwelling. The asthenospheric upwelling may contain fluids that ascend into the crust through some channels, such as the Tanlu fault zone, and reduce the effective normal stress on the fault plane to trigger the great 1668 Tancheng earthquake. Such dynamic processes are found around the Tanlu fault zone that is situated in the westernmost part of the BMW



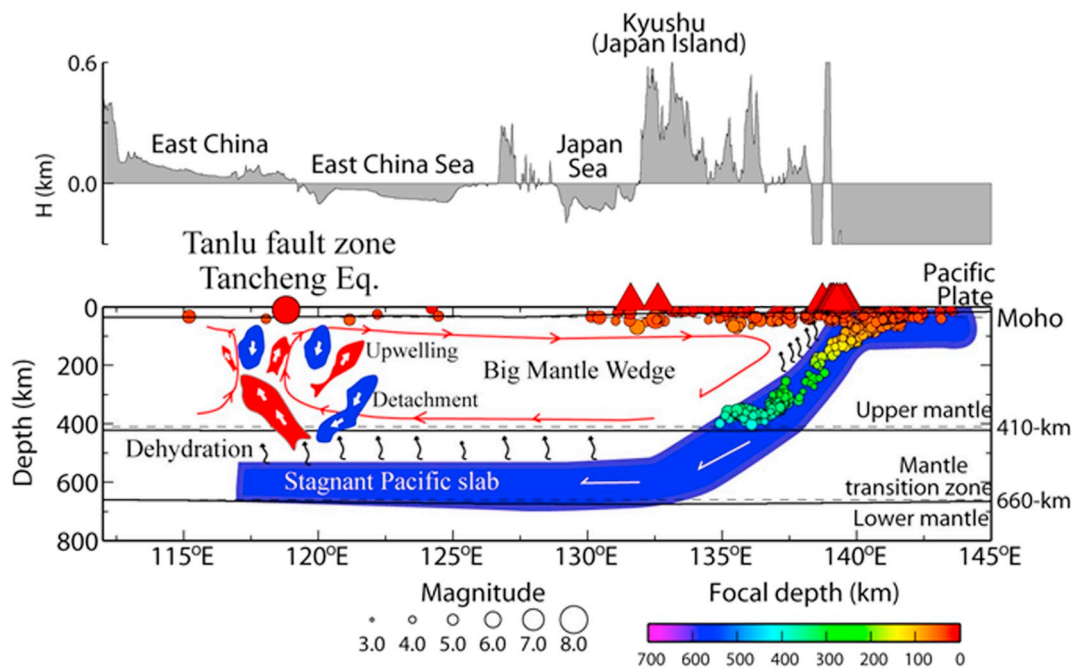


**Fig. 13.** A schematic diagram showing the mantle structure and dynamics along an east-west profile passing through the Tanlu fault zone and epicenter of the 1668  $M$  8.5 Tancheng earthquake (the biggest red dot). A big mantle wedge (BMW) has formed above the subducted Pacific slab that is stagnant in the MTZ under East Asia (e.g., Lei and Zhao, 2005; Zhao et al., 2007, 2009; Zhao and Tian, 2013; Lei et al., 2018b). Corner flow in the BMW and deep slab dehydration may lead to hot and wet mantle upwelling (red patches with white upward arrows). Downwelling (blue patches with white downward arrows) could be caused by lithospheric delamination due to thermal erosion. The mantle convection under the Tanlu fault zone includes both upwelling and downwelling. The color dots are earthquakes along the cross-section. The red triangles denote active volcanoes in the Japanese Islands. The dashed gray lines denote the Moho, 410 km and 660 km discontinuities from the IASP91 1-D velocity model (Kennett and Engdahl, 1991), whereas the solid black lines denote the three discontinuities revealed by several studies (Flanagan and Shearer, 1998; Laske et al., 2012; He et al., 2014; Li et al., 2014; Teng et al., 2014). The black curved arrows above the slab denote the slab dehydration, whereas the red arrows in the BMW denote mantle flow directions. The white arrows in the slab denote the moving direction of the subducting Pacific slab. (For interpretation of the references to color in this figure legend, the reader is referred to the web version of this article.)

(Fig. 13) (e.g., Lei and Zhao, 2005; Zhao et al., 2007, 2009; Zhao and Tian, 2013; Lei et al., 2018b). Similar BMW structures, such as broad high-V anomalies in the MTZ and low-V anomalies in the upper mantle, are also found under eastern Tibet (Lei et al., 2019). Therefore, we deem that mantle convection in the BMW is not a simple upwelling flow but has both upwelling and downwelling around the Tanlu fault zone. In NE China, a recent model of Pn anisotropic tomography revealed a complicated, east-west oriented, horizontal flow in the BMW, though the Pn model is limited to a thin horizontal layer in the uppermost mantle (Du and Lei, 2019). However, our present high-resolution 3-D tomographic model reveals complicated vertical flows containing both upwelling and downwelling around the Tanlu fault zone in the BMW (Figs. 12 and 13), which is supported by geochemical studies showing the existence of early Cretaceous volcanic rocks in broad areas along the Tanlu fault zone in Shandong province (e.g., Qiu et al., 1996).

## 5. Conclusions

Using a large number of high-quality teleseismic P-wave travel-time data, we obtain a new model of upper-mantle tomography around the Tanlu fault zone. Our results reveal significant lateral heterogeneities in the upper mantle under the study region. Prominent low-V anomalies are imaged above 200 km depth southwest of the 1668 Tancheng earthquake ( $M$  8.5) and at 200–470 km depths to the northeast, whereas some high-V anomalies are visible at 100–500 km depths. These results indicate that the NCC destruction could be caused by the lithospheric delamination and thermal erosion due to the hot and wet mantle upwelling in the BMW. In the lower part of the MTZ, high-V anomalies are visible, suggesting that the stagnant Pacific slab has reached under the Tanlu fault zone. Based on these findings, we propose that complicated vertical flows, containing both upwelling and

downwelling, exist in the BMW around the Tanlu fault zone. Under the source zone of the 1668 Tancheng earthquake, intermittent low-V anomalies extend down to the MTZ, suggesting that the great earthquake generation could be related to fluids ascending with the hot and wet mantle upwelling in the BMW.

## Acknowledgements

This work was partially supported by the Dream Project of MOST of China (Grant nos. 2016YFC0600408 and 2018YFC1504103), the National Natural Science Foundation of China (NSFC) (41530212 and 41674091), and the Tanlu Fault Zone Special Grant (TYZ20160111). The seismic waveform data recorded by the Chinese provincial seismic networks used in this study were provided by the Data Management Centre of the China National Seismic Network at the Institute of Geophysics (doi:10.11998/SeisDmc/SN) (Zheng et al., 2010), China Earthquake Administration, and the Shandong, Jiangsu, Anhui, and Shanghai Earthquake Administrations. We thank Drs. You Tian and Liang Zhao for providing their tomographic models for the comparison with our new model. The GMT software package distributed by Wessel and Smith (1995) is used for making the figures. Prof. Vernon Cormier (the Editor) and three anonymous referees provided thoughtful review comments and suggestions that have improved this paper.

## References

- Bruhn, R., Schultz, R., 1996. Geometry and slip distribution in normal fault systems: implications for mechanics and fault-related hazards. *J. Geophys. Res.* 101, 3401–3412.
- Cadek, O., Yuen, D.A., Steinbach, V., Chopelas, A., Matyska, C., 1994. Lower mantle thermal structural deduced from seismic tomography, mineral physics and numerical modeling. *Earth Planet. Sci. Lett.* 121, 385–402.

- Cao, G., Dong, N., 1987. A preliminary study on Decollement nappes in the Tancheng-Lujiang fault zone, Shandong Province. *Jilin Geol.* 2, 1–6.
- Chao, H., Li, J., Cui, Z., Zhao, Q., 1997. Mode of motion of the Holocene fault in Weifang-Jiashan segment of the Tanlu fault zone and earthquake-generating model. *J. Seismol. Res.* 20 (2), 218–226.
- Chen, P., 1988. The age and pattern of the great translations of the Tanlu fault zone. *Chin. Sci. Bull.* 33 (4), 289–293.
- Chen, L., Zheng, T., Xu, W., 2006. A thinned lithospheric image of the Tanlu fault zone, eastern China: constructed from wave equation based receiver function migration. *J. Geophys. Res.* 111, B09312. <https://doi.org/10.1029/2005JB003974>.
- Chen, L., Cheng, C., Wei, Z., 2009. Seismic evidence for significant lateral variations in lithospheric thickness beneath the central and western North China Craton. *Earth Planet. Sci. Lett.* 286, 171–183.
- Chen, C., Zhao, D., Tian, Y., Wu, S., Hasegawa, A., Lei, J., Park, J., Kang, L., 2017. Mantle transition zone, stagnant slab and intraplate volcanism. *Geophys. J. Int.* 209, 68–85.
- Deng, Q., Zhang, P., Ran, R., Yang, X., Min, W., Chu, Q., 2002. Basic characteristics of active tectonics of China. *Sci. China Earth Sci.* 32 (12), 1020–1031.
- Du, M., Lei, J., 2019. Pn anisotropic tomography of Northeast China and its implications to mantle dynamics. *J. Asian Earth Sci.* 171, 334–347.
- England, P., Houseman, G., 1986. Finite strain calculations of continental deformation: comparison with the India-Asia collision zone. *J. Geophys. Res.* 91, 3664–3676.
- England, P., Molnar, P., 1997. Active deformation of Asia: from kinematics to dynamics. *Science* 278, 647–650.
- Fan, W., Zhang, H., Baker, J., Jarvis, K., Mason, P., Menzies, M., 2000. On and off the North China Craton: where is the Archaean keel? *J. Petrol.* 41, 933–950.
- Flanagan, M., Shearer, P., 1998. Global mapping of topography on transition zone velocity discontinuities by stacking SS precursors. *J. Geophys. Res.* 103, 2673–2692.
- Fouch, M., Rondenay, S., 2006. Seismic anisotropy beneath stable continental interiors. *Phys. Earth Planet. Inter.* 158, 292–320.
- Fukao, Y., Obayashi, M., 2013. Subducted slabs stagnant above, penetrating through, and trapped below the 660 km discontinuity. *J. Geophys. Res. Solid Earth* 118, 5920–5938.
- Gao, W., Li, J., Sun, Z., 1980. Formation and evolution of the Yihe-Shuhe continental rift. *Seismol. Geol.* 12, 11–18.
- Gao, S., Rudnick, R., Carlson, R., McDonough, W., Liu, Y., 2002. Re-Os evidence for replacement of ancient mantle lithosphere beneath the North China Craton. *Earth Planet. Sci. Lett.* 198, 307–322.
- Gou, T., Zhao, D., Huang, Z., Wang, L., 2019. Aseismic deep slab and mantle flow beneath Alaska: insight from anisotropic tomography. *J. Geophys. Res.* 124, 1700–1724.
- Griffin, W.L., Zhang, A.D., O'Reilly, S.Y., Ryan, G., 1998. Phanerozoic evolution of the lithosphere beneath the Sino-Korean Craton. In: Flower, M., Chung, S.L., Lo, C.H., Lee, T.Y. (Eds.), *Mantle Dynamics and Plate Interactions in East Asia: American Geophysical Union Geodynamics Series*. 27. pp. 107–126.
- Guo, Z., 1987. The formation, evolution, movement, and rotation of the Tanlu fault zone. *Shandong Geology* 3 (1), 51–62.
- He, L., 2017. Wet plume atop of the flattening slab: insight into intraplate volcanism in East Asia. *Phys. Earth Planet. Inter.* 269, 29–39.
- He, R., Shang, X., Yu, C., Zhang, H., van der Hilst, R., 2014. A unified map of Moho depth and Vp/Vs ratio of continental China by receiver function analysis. *Geophys. J. Int.* 199, 1910–1918.
- He, P., Lei, J., Yuan, X., Xu, X., Xu, Q., Liu, Z., Mi, Q., Zhou, L., 2018. Lateral Moho variations and the geometry of the Main Himalayan thrust beneath the Nepal Himalayan orogeny revealed by teleseismic receiver functions. *Geophys. J. Int.* 214, 1004–1017.
- Hickman, S., Sibson, R., Bruhn, R., 1995. Introduction to special section: mechanical involvement of fluids in faulting. *J. Geophys. Res.* 100, 12831–12840.
- Honda, S., Yuen, D.A., Balachandrar, S., Reuteler, D., 1993. Three-dimensional instabilities of mantle convection with multiple phase transitions. *Science* 259, 1308–1311.
- Huang, J., Zhao, D., 2004. Crustal heterogeneity and seismotectonics of the region around Beijing, China. *Tectonophysics* 385, 159–180.
- Huang, J., Zhao, D., 2006. High-resolution mantle tomography of China and surrounding regions. *J. Geophys. Res.* 111, B09305. <https://doi.org/10.1029/2005JB004066>.
- Huang, Z., Wang, P., Zhao, D., Wang, L., Xu, M., 2014. Three-dimensional P-wave azimuthal anisotropy in the lithosphere beneath China. *J. Geophys. Res.* 119, 5686–5712.
- Huang, Z., Zhao, D., Liu, X., 2015. On the trade-off between seismic anisotropy and heterogeneity: numerical simulations and application to Northeast Japan. *J. Geophys. Res.* 120, 3255–3277.
- Hung, S., Shen, Y., Chiao, L., 2004. Imaging seismic velocity structure beneath the Iceland hot spot: a finite frequency approach. *J. Geophys. Res.* 109, B08305. <https://doi.org/10.1029/2003JB002889>.
- Ishe, M., Oda, H., 2005. Three-dimensional structure of P-wave anisotropy beneath the Tohoku district, Northeast Japan. *J. Geophys. Res.* 110, B07304. <https://doi.org/10.1029/2004JB003599>.
- Jiang, G., Zhang, G., Zhao, D., Lu, Q., Li, H., Li, X., 2015. Mantle dynamics and cretaceous magmatism in east-central China: insight from teleseismic tomograms. *Tectonophysics* 664, 256–268.
- Johnson, P.A., McEvilly, T.V., 1995. Parkfield seismicity: fluid-driven? *J. Geophys. Res.* 100, 12937–12950.
- Karato, S., Jung, H., Katayama, I., Skemer, P., 2008. Geodynamic significance of seismic anisotropy of the upper mantle: new insights from laboratory studies. *Annu. Rev. Earth Planet. Sci.* 36, 59–95.
- Kennett, B.L.N., Engdahl, R., 1991. Travel times for global earthquake location and phase identification. *Geophys. J. Int.* 105, 429–465.
- Laske, G., Masters, G., Ma, Z., Pasyanos, M., 2012. CRUST1.0: An updated global model of Earth's crust. *Geophysical Research Abstracts* 14, EGU2012-3743-1.
- Lei, J., 2012. Upper-mantle tomography and dynamics beneath the North China Craton. *J. Geophys. Res.* 117, B06313. <https://doi.org/10.1029/2012JB009212>.
- Lei, J., Zhao, D., 2005. P-wave tomography and origin of the Changbai intraplate volcano in Northeast Asia. *Tectonophysics* 397, 281–295.
- Lei, J., Zhao, D., 2006. Global P-wave tomography: on the effect of various mantle and core phases. *Phys. Earth Planet. Inter.* 154, 44–69.
- Lei, J., Zhao, D., 2007. Teleseismic P-wave tomography and the upper mantle structure of the central Tien Shan orogenic belt. *Phys. Earth Planet. Inter.* 162, 165–185.
- Lei, J., Zhao, D., 2009. Structural heterogeneity of the Longmenshan fault zone and the mechanism of the 2008 Wenchuan earthquake (Ms 8.0). *Geochim. Geophys. Geosyst.* 10, Q10010. <https://doi.org/10.1029/2009GC002590>.
- Lei, J., Xie, F., Lan, C., Xing, C., Ma, S., 2008. Seismic images under the Beijing region inferred from P and PmP data. *Phys. Earth Planet. Inter.* 168, 134–146.
- Lei, J., Xie, F., Mishra, O.P., Lu, Y., Zhang, G., Li, Y., 2012. The 2011 Yingjiang, China, earthquake: a volcano-related fluid-driven earthquake? *Bull. Seismol. Soc. Am.* 102 (1), 417–425.
- Lei, J., Zhang, G., Xie, F., 2014. The 20 April 2013 Lushan, Sichuan, mainshock, and its aftershock sequence: tectonic implications. *Earthquake Sci.* 27 (1), 15–25.
- Lei, J., Zhao, D., Xu, X., Du, M., Zhang, G., Sun, C., Mi, Q., Lu, M., Yang, Y., He, J., Zhang, B., Tian, F., 2018a. Deep structure of the Longmenshan fault zone and mechanism of the 2008 Wenchuan earthquake. *Chin. Sci. Bull.* 63, 1906–1916.
- Lei, J., Zhao, D., Xu, Y., Fan, Q., Mi, Q., Du, M., Lu, M., 2018b. Is there a gap in the stagnant Pacific slab in the mantle transition zone under the Changbaishan volcano? *Acta Petrol. Sin.* 34 (1), 13–22.
- Lei, J., Zhao, D., Xu, X., Xu, Y., Du, M., 2019. Is there a big mantle wedge structure under eastern Tibet? *Phys. Earth Planet. Inter.* 292, 100–113.
- Li, C., van der Hilst, R., 2010. Structure of the upper mantle and mantle transition zone beneath Southeast Asia from traveltime tomography. *J. Geophys. Res.* 115, B07308.
- Li, J., Chao, H., Cui, Z., Zhao, Q., 1994. Segmentation of active fault along the Tancheng-Lujiang fault zone. *Seismol. Geol.* 16 (2), 121–126.
- Li, S., Lai, X., Liu, B., Wang, Z., He, J., Sun, Y., 2011. Differences in lithospheric structures between two sides of Taihang Mountain obtained from the Zhucheng-Yichuan deep seismic sounding profile. *Sci. China Earth Sci.* 54, 871–880.
- Li, Y., Gao, M., Wu, Q., 2014. Crustal thickness map of the Chinese mainland from teleseismic receiver functions. *Tectonophysics* 611, 51–60.
- Liu, X., Zhao, D., 2016. Seismic velocity azimuthal anisotropy of the Japan subduction zone: constraints from P and S wave traveltimes. *J. Geophys. Res.* 121, 5086–5115.
- Liu, B., Feng, S., Ji, J., Shi, J., Tan, Y., Li, Y., 2015. Fine lithosphere structure beneath the middle-southern segment of the Tan-Lu fault zone. *Chinese J. Geophys.* 58 (5), 1610–1621 (in Chinese).
- Long, M., Becker, T., 2010. Mantle dynamics and seismic anisotropy. *Earth Planet. Sci. Lett.* 297, 341–354.
- Lu, H., Yu, H., Ding, Y., Zhang, Q., 1983. Changing stress field in the middle segment of the Tan-Lu fault zone, eastern China. *Tectonophysics* 98, 253–270.
- Machetel, P., Weber, P., 1991. Intermittent layered convection in a model mantle with an endothermal phase change at 670 km. *Nature* 350, 55–57.
- Menzies, M.A., Fan, W.M., Zhang, M., 1993. Palaeozoic and Cenozoic lithoprobes and the loss of N120 km of Archaean lithosphere, Sino-Korean craton, China. In: Prichard, H.M., Alabaster, T., Harris, N.B.W., Neary, C.R. (Eds.), *Magmatic Processes and Plate Tectonics: Geol. Soc. Spel. Pub.* vol. 76. pp. 71–78.
- Miller, S.A., 1996. Fluid-mediated influence of adjacent thrusting on the seismic cycle at Parkfield. *Nature* 382, 799–802.
- Mishra, O.P., Zhao, D., 2003. Crack density, saturation rate and porosity at the 2001 Bhuj, India, earthquake hypocenter: a fluid-driven earthquake? *Earth Planet. Sci. Lett.* 212, 393–405.
- Molnar, P., Tapponnier, P., 1975. Cenozoic tectonics of Asia: effects of a continental collision. *Science* 189, 419–426.
- Obayashi, M., Yoshimitsu, J., Fukao, Y., 2009. Tearing of stagnant slab. *Science* 324, 1173–1175.
- Okay, A., Sengor, A., 1992. Evidence for intracontinental thrust-related exhumation of the ultra-high-pressure rocks in China. *Geology* 20, 411–414.
- Paige, C., Saunders, M., 1982. LSQR: an algorithm for sparse linear equations and sparse least squares. *Association of Computer and Mathematical Transaction on Mathematical Software* 8, 43–71.
- Qiu, J., Wang, D., Zhou, J., Zeng, J., 1996. Geology, geochemistry and genesis of the Mesozoic shoshonitic volcanic rocks in Shandong province. *Earth Sci. J. China Univ. Geosci.* 21, 546–552.
- Shen, X., Zhou, H., Kawakatsu, H., 2008. Mapping the upper mantle discontinuities beneath China with teleseismic receiver functions. *Earth Planets Space* 60, 713–719.
- Sibson, R., 1982. Fault zone models, heat flow and the depth distribution of earthquakes in the continental crust of the United States. *Bull. Seismol. Soc. Am.* 72, 151–163.
- Sibson, R., 1992. Implications of fault-value behavior for rupture nucleation and recurrence. *Tectonophysics* 211, 283–293.
- Song, Z., Zhang, G., Liu, J., Yin, J., Xue, Y., Song, X., 2011. *Global Earthquake Catalog*. Seismological Press, Beijing, pp. 1–450.
- Teng, J., Deng, Y., Badal, J., Zhang, Y., 2014. Moho depth, seismicity and seismogenic structure in China mainland. *Tectonophysics* 627, 108–121.
- Tian, Y., Zhao, D., 2012. Seismic anisotropy and heterogeneity in the Alaska subduction zone. *Geophys. J. Int.* 190, 629–649.
- Tian, Y., Zhao, D., 2013. Reactivation and mantle dynamics of North China Craton: insight from P-wave anisotropy tomography. *Geophys. J. Int.* 195, 1796–1810.
- Tian, Y., Zhao, D., Sun, R., Teng, J., 2009. Seismic imaging of the crust and upper mantle beneath the North China Craton. *Phys. Earth Planet. Inter.* 172, 169–182.
- VanDecar, J., Crosson, R., 1990. Determination of teleseismic relative phase arrival times using multi-channel cross-correlation and least squares. *Bull. Seismol. Soc. Am.* 80, 150–169.



- Wan, T., Zhu, M., 1996. The maximum sinistral left-slip and its forming age of Tancheng-Lujiang fault zone. *Geol. J. Univ.* 2 (1), 14–27.
- Wang, K., Bilek, S., 2011. Do subducting seamounts generate or stop large earthquakes? *Geology* 39 (9), 819–822.
- Wang, J., Zhao, D., 2008. P-wave anisotropic tomography beneath Northeast Japan. *Phys. Earth Planet. Inter.* 170, 115–133.
- Wang, X., et al., 2000. The Tanlu Fault Zone. Geological press, Beijing, pp. 1–374.
- Wei, W., Xu, J., Zhao, D., Shi, Y., 2012. East Asia mantle tomography: new insight into plate subduction and intraplate volcanism. *J. Asian Earth Sci.* 60, 88–103.
- Wei, W., Zhao, D., Xu, J., Zhou, B., Shi, Y., 2016. Depth variations of P-wave azimuthal anisotropy beneath Mainland China. *Sci. Rep.* 6, 29614. <https://doi.org/10.1038/srep29614>.
- Wessel, P., Smith, W., 1995. New version of the generic mapping tools (GMT) version 3.0 released. *EOS Transaction AGU* 76, 329.
- Wu, F., Zhang, Y., Fang, Z., Zhang, S., 1981. On the activity of the Tancheng-Lujiang fault zone in China. *Seismol. Geol.* 3 (4), 15–26.
- Wu, F., Lin, J., Wilde, S., Zhang, X., Yang, J., 2005. Nature and significance of the early Cretaceous giant igneous event in eastern China. *Earth Planet. Sci. Lett.* 233, 103–119.
- Wu, F., Zhang, Y., Yang, J., Xie, L., Yang, Y., 2008. Zircon U-Pb and Hf isotopic constraints on the early Archean crustal evolution in Anshan of the North China Craton. *Precambrian Res.* 167, 339–362.
- Xu, J., 1984. The Tancheng-Lujiang wrench fault system. In: *Forum on Structural Geology*. 3. Geological Press, Beijing, pp. 18–23.
- Xu, J., 1993. The Tancheng-Lujiang Wrench Fault System. John Wiley and Sons Ltd, New York, pp. 1–300.
- Xu, Y., 2001. Thermotectonic destruction of the Archean lithospheric keel beneath eastern China: evidence, timing, and mechanism. *Phys. Chem. Earth A* 26, 747–757.
- Xu, J., Ma, G., 1992. Review of ten years (1981–1991) of research on the Tancheng-Lujiang fault zone. *Geol. Rev.* 38 (4), 316–324.
- Xu, P., Zhao, D., 2009. Upper-mantle velocity structure beneath the North China Craton: implications for lithospheric thinning. *Geophys. J. Int.* 177, 1279–1283.
- Xu, J., Zhu, G., Tong, W., Cui, K., Liu, Q., 1987. Formation and evolution of the Tancheng-Lujiang wrench fault system: a major shear system to the northeast of the Pacific Ocean. *Tectonophysics* 134, 273–310.
- Xu, X., Ma, X., Deng, Q., 1993. Neotectonic activity along the Shanxi rift system, China. *Tectonophysics* 219, 305–325.
- Yang, J., Zhao, L., Kaus, B., Lu, G., Wang, K., Zhu, R., 2018. Slab-triggered wet upwellings produce large volumes of melt: insights into the destruction of the North China Craton. *Tectonophysics* 746, 266–279.
- Ye, G., Wei, W., Jin, S., Jing, J., 2009. Study of electrical structure and its geological meanings of the middle part of Tancheng-Lujiang fault zone. *Chinese J. Geophys.* 52 (11), 2818–2825 (in Chinese).
- Yin, A., 2000. Mode of Cenozoic east-west extension in Tibet suggesting a common origin of rifts in Asia during the Indo-Asian collision. *J. Geophys. Res.* 105, 21745–21759.
- Zhang, Y., Shi, W., Dong, S., 2003. Cenozoic deformation history of the Tancheng-Lujiang fault zone, North China and dynamic implications. *Island Arc* 12 (3), 281–293.
- Zhang, J., Zhao, G., Xiao, Q., Tang, J., 2010. Analysis of electric structure of the central Tan-Lu fault zone (Yi-Shu fault zone) and seismogenic condition. *Chinese J. Geophys.* 53 (3), 605–611 (in Chinese).
- Zhao, D., 2001. Seismic structure and origin of hotspots and mantle plumes. *Earth Planet. Sci. Lett.* 192, 251–265.
- Zhao, D., Lei, J., 2004. Seismic ray path variations in a 3-D global velocity model. *Phys. Earth Planet. Inter.* 141, 153–166.
- Zhao, D., Tian, Y., 2013. Changbai intraplate volcanism and deep earthquakes in East Asia: a possible link? *Geophys. J. Int.* 195, 706–724.
- Zhao, D., Hasegawa, A., Kanamori, H., 1994. Deep structure of Japan subduction zone as derived from local, regional, and teleseismic events. *J. Geophys. Res.* 99, 22313–22329.
- Zhao, D., Kanamori, H., Negishi, H., 1996. Tomography of the source area of the 1995 Kobe earthquake: evidence for fluids at the hypocenter? *Science* 274, 1891–1894.
- Zhao, D., Mishra, O.P., Sanda, R., 2002. Influence of fluids and magma on earthquakes: seismological evidence. *Phys. Earth Planet. Inter.* 132, 249–267.
- Zhao, D., Maruyama, S., Omori, S., 2007. Mantle dynamics of Western Pacific and East Asia: insight from seismic tomography and mineral physics. *Gondwana Res.* 11, 120–131.
- Zhao, D., Tian, Y., Lei, J., Liu, L., Zheng, S., 2009. Seismic image and origin of the Changbai intraplate volcano in East Asia: role of big mantle wedge above the stagnant Pacific slab. *Phys. Earth Planet. Inter.* 173, 197–206.
- Zhao, L., Allen, R., Zheng, T., Zhu, R., 2012. High-resolution body wave tomography models of the upper mantle beneath eastern China and the adjacent areas. *Geochim. Geophys. Geosyst.* 13, Q06007. <https://doi.org/10.1029/2012GC004119>.
- Zhao, D., Yu, S., Liu, X., 2016. Seismic anisotropy tomography: new insight into subduction dynamics. *Gondwana Res.* 33, 24–43.
- Zheng, X., Yao, Z., Liang, J., Zheng, J., 2010. The role played and opportunity provided by IGP DMC of China National Seismic Network in Wenchuan earthquake disaster relief and researches. *Bull. Seismol. Soc. Am.* 100, 2866–2872.
- Zhou, Z., Lei, J., 2016. Pn anisotropic tomography and mantle dynamics beneath China. *Phys. Earth Planet. Inter.* 257, 193–204.
- Zhu, G., Song, C., Wang, D., Liu, G., Xu, J., 2001. Studies on  $^{40}\text{Ar}/^{39}\text{Ar}$  geochronology of strike-slip time of the Tan-Lu fault zone and their tectonic implications. *Sci. China (Ser. D)* 44 (11), 1002–1009.
- Zhu, G., Liu, G., Niu, M., Song, C., Wang, D., 2003. Transcurrent movement and genesis of the Tan-Lu fault zone. *Geol. Bull. China* 22 (3), 200–207.
- Zhu, G., Hu, Z., Chen, Y., Niu, M., Xie, C., 2008. Evolution of Early Cretaceous extensional basin in the eastern North China craton and its implication for the craton destruction. *Geol. Bull. China* 27 (10), 1594–1604.
- Zhu, R., Chen, L., Wu, F., Liu, J., 2011. Timing, scale and mechanism of the destruction of the North China Craton. *Sci. China Earth Sci.* 54, 789–797.
- Zhu, R., Xu, Y., Zhu, G., Zhang, H., Xia, Q., Zheng, T., 2012. Destruction of the North China Craton. *Sci. China Earth Sci.* 42 (8), 1135–1159.